CCFE
CULHAM CENTRE FOR FUSION ENERGY

UK Atomic Energy Authority

UKAEA-CCFE-PR(23)101

Yulin Zhou, Benjamin Dudson, Fulvio Militello, Kiven Verhaegh, Omkar Myatra

Investigation of the role of hydrogen molecules in 1D simulation of divertor detachment

Investigation of the role of hydrogen molecules in 1D simulation of divertor detachment

Yulin Zhou, Benjamin Dudson, Fulvio Militello, Kiven Verhaegh, Omkar Myatra

This is a preprint of a paper submitted for publication in Plasma Physics and Controlled Fusion

Investigation of the role of hydrogen molecules in 1D simulation of divertor detachment

Yulin Zhou[1,3], Benjamin Dudson[1,4], Fulvio Militello[2], Kiven Verhaegh[2] and Omkar Myatra[2]

[1] York Plasma Institute, Department of Physics, University of York, YO10 5DQ, UK

[2] United Kingdom Atomic Energy Authority, Culham Centre for Fusion Energy, Culham Science Centre, Abingdon, Oxon, OX14 3DB, United Kingdom

[3]Southwestern Institute of Physics, Chengdu 610041, China

[4]Lawrence Livermore National Laboratory, 7000 East Ave, Livermore, CA 94550, USA

Abstract

The role of neutral and charged hydrogenic molecules in detached regimes of tokamak plasmas is investigated using simplified 1D parallel numerical models. Using MAST-Upgrade like conditions, simulations are implemented to study the rollover of target flux Γ in upstream density scan and target temperature scan. It is found that if H_2 and $H_2{}^+$ are considered in simulations a lower target temperature and a larger upstream density will be required to trigger the divertor detachment under the same input power and particle flux, and the critical detachment threshold is found to be $\frac{p_{up}}{P_{recl}} \sim 8.1\ N/MW$ at rollover. Molecule–plasma interactions are found to be as crucial as atom–plasma interactions during divertor detachment, both of which account for the main plasma momentum loss. Further analysis of the momentum loss decomposition shows molecule-plasma elastic collision dominates molecule-plasma interactions, while molecular charge exchange cannot effectively reduce plasma momentum. In terms of H_{alpha} emission, a strong rise of H_{alpha} signal could be found due to molecular excitation channels when the upstream density further increases after rollover.

Keywords: tokamak, divertor detachment, molecules, plasma momentum loss, H_{alpha} emission, SD1D

A. Introduction

Impurity induced detachment discharge and density ramp detachment discharge are two important ways to realize the divertor detachment [1][2]. According to the first detachment regime, the divertor volume is cooled down mainly due to the radiation of impurity, which is generated by plasma-material interactions (e.g. C, W) [3] or impurity seeding (e.g. N_2, Ne) [4]. During a density ramp discharge, molecular hydrogen H_2 is injected into the divertor volume through gas puffing and therefore creates an increasing density of neutral particles, which interacts with the plasma flux moving towards the target and cools it down. Despite general consensus on the importance of impurities and neutral particles on divertor detachment, uncertainties remain in the details of how the molecule species ($H_2, H^-, H_2{}^+$and $H_3{}^+$) influence divertor physics before and after flux rollover is achieved, and how these in turn affect the conditions to achieve divertor detachment [5][6]. For example, the effects of molecular processes (e.g. molecular charge exchange, molecular assisted recombination (MAR), molecular assisted ionization (MAI)) on the momentum and power loss in divertor volume [7][8], the effect of plasma recycling with different wall and target materials [9] [10], and the importance of hydrogen emission radiation [11] in different detachment discharge regimes are all active areas of research. These studies are crucial for

understanding the atomic and molecular physics in divertor volume, and will be helpful to better control the divertor detachment in experiment.

The sophisticated 2D edge plasma transport codes, e.g. SOLPS, EDGE2D [12][13], have been widely used for studying edge plasma phenomena e.g. divertor detachment, but they are often too complex for easy interpretation of the physics involved. The simplified analytic [2][14] and 1D computational model (e.g. [15][16][17]) could provide more details of the underlying processes of edge plasma. This paper aims to explore the dynamics of molecule species and their effects on the detachment process with a BOUT++ module named SD1D[15] (section B.1). SD1D is a time-dependent code and could be used to investigate the importance of power and momentum loss to the detachment process, the profile variation in different detachment discharge regimes, feedback control of detachment, and the dynamics of different particle species during the detachment process [15]. In [15] only the dynamics of plasma and neutral atom was included in the SD1D model. To investigate the effects of molecule species, we have upgraded the SD1D model: the dynamics of H_2 and $H_2{}^+$, the collisional reactions related to molecule species, and the emission radiation via molecule channels ($H_2, H^-, H_2{}^+$) have been added to the physical model (section B.2). The reaction rate coefficients and hydrogen emissivity used in the upgraded SD1D are shown in section C. These coefficients are calculated by the data from the EIRENE-Amjuel database [18], another improvement over the original SD1D code used in [15]. With the upgraded SD1D, we analyse the cases with and without carbon impurity in the MAST-Upgrade conditions, the variations of plasma ion flux to the target in different recycling conditions, the critical detachment threshold, the importance of molecular species on plasma momentum loss, and H_{alpha} emission in different excitation channels as shown in section D.

B. The SD1D model

1. The physical model of old SD1D version

SD1D uses a 1D time dependent fluid model [2][17], which evolves the plasma density n, parallel momentum density $m_i n v_\parallel$ and static pressure $p = 2enT$. The equations are shown below [15]:

$$\frac{\partial n}{\partial t} = -\nabla \cdot \left[\mathbf{b} v_{||} n\right] + S_n - S \tag{1a}$$

$$\frac{\partial}{\partial t}\left(\frac{3}{2}p\right) = -\nabla \cdot \mathbf{q}_e + v_{||}\partial_{||} p + S_E - E - R \tag{1b}$$

$$\frac{\partial}{\partial t}\left(m_i n v_{||}\right) = -\nabla \cdot \left[m_i n v_{||} \mathbf{b} v_{||}\right] - \partial_{||} p - F \tag{1c}$$

Where $\partial_\parallel = \boldsymbol{b} \cdot \nabla$, the heat flux is $\boldsymbol{q}_e = \frac{5}{2} p \boldsymbol{b} v_\parallel - \kappa_\parallel \boldsymbol{\partial}_\parallel T_e$, and thermal conduction coefficient is $\kappa = \kappa_0 T^{\frac{5}{2}}$. The ion and electron temperatures are assumed to be equal and isotropic: $T_e = T_i$. In eq.1a, S_n is the external particle source evolved by a proportional-integral (PI) feedback controller. S shows the particle sources and sinks caused by collisional reactions like ionisation and recombination. In eq.1b, S_E represents an external source of power that keeps injecting energy with a fixed rate into a volume above X-point; E presents energy exchange due to plasma-neutral interactions; R is radiation power generated by hydrogen excitation and impurity radiation.

The equations of atom density n_n, atom parallel momentum $n_n v_{\parallel n}$ and atom static pressure $n_n T_n$ are similar to eq.1a – eq.1c. Since the magnetic field is unable to confine the neutrals, the atoms can be transported across the magnetic field and spread upstream. To model this process, SD1D gives an effective parallel velocity to atoms which is the sum of a parallel flow and parallel projection of a perpendicular diffusion [15]:

$$v_n = v_{||n} - \left(\frac{B_\phi}{B_\theta}\right)^2 \frac{\partial_{||} p_n}{\nu} \tag{2}$$

Where total atom collision frequency ν is calculated by the sum of charge exchange rate, ionisation rate and neutral-neutral collision rate and the cross-field neutral diffusion multiplier (field-line pitch) $(\frac{B_\phi}{B_\theta})^2$ is equal to 10 in the simulations shown here.

Only atom particle species are included in the original neutral model of SD1D, while volumetric processes involving molecule particle species are not considered. As discussed in section A, molecules can be a crucial part of divertor plasma dynamics, especially for the divertor detachment. To study the effects of molecules with SD1D, it is necessary to create a molecule model in SD1D. An impurity model '*atomic++coronal*', based on coronal equilibrium, is applied in SD1D [19]. It is able to provide impurity radiation power (i.e. carbon) with a fixed impurity fraction, through fetching and using data from ADAS database [20].

The Bohm boundary conditions are used at the target, where the parallel plasma velocity $v_\parallel \geq c_s$. The plasma density and pressure boundaries are 'free', so that they are extrapolated into the boundary. The temperature gradient at the sheath entrance is set to zero, and the energy flux corresponds to a sheath heat transmission of $q = \gamma n T c_s$ [15], where the sheath transmission coefficient γ is equal to 6. As for recycling process, SD1D sets the recycling fraction of ion flux to the target with $f_{recl} = \frac{\Gamma_{recl}}{\Gamma_{ion}^t} = 0.99$, which represents that 99% of plasma ion flux to target Γ_{ion}^t is recycled and becomes the neutral flux Γ_{recl} (atoms and molecules) in the final grid point at target [15].

2. The upgrades of SD1D

In the previous version of SD1D, only atomic collisional and radiative reactions were included, while molecular processes were neglected. To better investigate the physics of divertor detachment, an important upgrade of the SD1D model was carried out by adding a molecule model, including a hydrogen molecule model labelled 'm' and a charged molecule model labelled 'H_2^+'. Like for the atom model, equations of molecule density n_m, parallel momentum $n_m v_{\parallel m}$ and static pressure $n_m T_m$ are also in the form of eq.1a –eq.1c. The terms of particle sinks, energy exchange E_m and friction force F_m are generated by the collisional reactions listed in Table 1, including non-dissociative ionisation, dissociation, molecular charge exchange and molecular activated recombination (MAR) via H^-. Following eq.2, a similar parallel velocity v_m is given to molecules in the current SD1D implementation, with the cross-field neutral diffusion $(\frac{B_\phi}{B_\theta})^2 = 10$. Differently from eq.2, the total molecule collision frequency is calculated by the sum of molecular charge exchange rate, non-dissociative ionisation rate and neutral-neutral collision rate.

Now the new model contains two neutral species, atom and molecule. According to the experiment in the divertors, both atoms and molecules are important plasma recycling channels [11]. Based on the original atomic recycling model [15], a new recycling channel H_2 has been included in SD1D. In section D, a comparison was made to study the influence of molecules on detachment physics with different recycling fractions.

Consistently with the atomic and neutral molecules equations a similar set of three equations for charged molecule H_2^+ is also added in SD1D: the sources, sinks and friction force in density, pressure and momentum equations are determined by dissociative excitation, molecular ionisation, dissociative ionisation, dissociative recombination and molecular charge exchange shown in Table 1 (reaction 4, 6, 7, 8 and 9)

As discussed in section B.1, Bohm boundary conditions are also used for H_2^+ at the target, where the parallel plasma velocity $v_{\parallel,H_2^+} \geq c_{s,H_2^+}$. The density and pressure boundaries of H_2

and H_2^+ are 'free'. The temperature gradient of H_2^+ at the sheath entrance is also zero, and the energy flux is related to a sheath heat transmission of $q_{H_2^+} = \gamma n_{H_2^+} T_{H_2^+} c_{s,H_2^+}$, where γ=6.

Table 1. List of collisional reactions (black) in the atom model and the reactions (blue) in the molecule model

Index	Reactions	Reaction types
1	$e + H \rightarrow 2e + H^+$	Ionization
2	$H^+ + H \rightarrow H + H^+$	Charge exchange
3	$H^+ + e \rightarrow H$	Recombination
4	$e + H_2 \rightarrow 2e + {H_2}^+$	Non-dissociative Ionization
5	$e + H_2 \rightarrow e + H + H$	Dissociation
6	$H^+ + H_2 \rightarrow {H_2}^+ + H$	Molecular charge exchange
7	$e + {H_2}^+ \rightarrow e + H^+ + H$	Dissociative excitation
8	$e + {H_2}^+ \rightarrow 2e + H^+ + H^+$	Dissociative ionization
9	$e + {H_2}^+ \rightarrow H + H$	Dissociative recombination
10	$H^+ + H_2 + e \rightarrow H + H + H$	MAR via H^-

In the original SD1D model, semi-analytic approximations [21][22] were used to calculate hydrogenic rates, such as rate coefficients of atom-plasma interactions and hydrogen emissivity. According to the approximations, however, the reaction rate coefficients for ionisation, recombination and charge exchange only depend on the electron temperature T_e. This, however, was not very precise since rate coefficients have a n_e dependence as well, which is particularly strong for the rate coefficient of recombination, ionisation, and dissociative recombination.

Taking into account the density dependence of the plasma-neutral interactions is important because the electron density in the divertor can significantly change depending on the operation conditions and is sensitive to the variation of upstream density, heat and particle flux. When divertor detachment is triggered by increasing upstream density, the peak electron density in the divertor will be several times larger than its peak density in attached conditions, while when fully detached the electron density at the target can reduce. Thus, it is essential to consider electron density variation in the calculation of rate coefficients and emissivity. To solve this issue, the 'Amjuel' database has been used in SD1D. Amjuel provides double polynomial fitting expression as a function of electron temperature and density to calculate rate coefficients of electron-atom, electron-ion and electron-molecule interactions (i.e. ionisation, dissociation, recombination and the reactions related to molecule) [18]. For the ion-atom, ion-molecule interactions (i.e. charge exchange), its double polynomial expression is a function of energies of the two collided particles [18].

Besides collisional reactions, the hydrogen emission radiation caused by atom-plasma or molecule-plasma interactions is also crucial for the divertor physics. It contributes a significant energy loss from the plasma in the divertor volume, and greatly affects the target flux in terms of particle and power balance. The previous SD1D version already considered hydrogen atomic excitation, but its hydrogen atom emissivity is just an empirical function of T_e. According to the discussion about rate coefficient fitting functions above, it is more precise and reliable to associate the emissivity with both T_e and n_e. Furthermore, there is no molecular excitation model included in the old version. Here, the hydrogen emissivity as a function of T_e and N_e can be modelled by the population coefficients from Amjuel. According the collisional and radiative models [23], there are 6 channels to generate excited atoms for hydrogen excitations. Direct excitation (via H) and recombination (via H^+) are atomic excitation channels. Dissociation (via H_2), dissociative recombination (via ${H_2}^+$ and ${H_3}^+$) and mutual neutralization (via H^-) are molecular excitation channels. Just as the channel's names imply, the radiative reactions always happen together with the corresponding collisional reactions.

The radiation power induced by every channels could be obtained by the following steps. I_{pq} is the emission intensity from state 'p' to 'q' and defined as

$$I_{pq} = N_e N_0 \chi_{pq}^{eff}, \quad (3)$$

$$\chi_{pq}^{eff} = R_{0p} A_{pq}, \quad (4)$$

$$R_{0p} = \frac{N_p}{N_e N_0}, \quad (5)$$

where χ_{pq}^{eff} is effective emission rate coefficient and R_{0p} represents the population coefficient of the excited hydrogen atom in state 'p' [18]; A_{pq} is the Einstein coefficient or possibility of transmitting from state 'p' to 'q' [24]; N_0 is the density of the reacting species which collides with electrons to generate atoms in the excited state 'p' (e.g for direct excitation N_0 represents the density of hydrogen atom). From eq. (3-5), we can get the emission intensity of the excited atom from state 'p' to 'q' in eq. 6.

$$I_{pq} = N_e N_0 \chi_{pq}^{eff} = N_e N_0 \times \frac{N_p}{N_e N_0} \times A_{pq} = N_p A_{pq} \quad (6)$$

Then multiplying I_{pq} with the energy gap between any two states E_{pq} [24], the radiation power by the excited atoms in a certain state 'p' is obtained by eq. 7.

$$Pow_{pq} = E_{pq} \times I_{pq} \quad (7)$$

Through sum up the radiation power over energy level transmissions (only Lyman series of p=2-6 is considered), the radiation power of an excitation channel can be written as:

$$Pow_{pq}^{channel} = \sum_{p=2}^{6} \sum_{q=p-1}^{5} E_{pq} N_p A_{pq} \quad (8)$$

Repeat the calculation for all the 6 excitation channels, and we can get the total hydrogen emission radiation power per volume (e.g in the unit $\mathrm{W/m^3}$) by summing up the radiation powers of all channels.

The dynamics of ${H_3}^+$ and H^- are not considered in the upgraded SD1D due to their tiny density and limited contribution to the energy loss in experiment [25][26]. But the emission radiation via H^- is still added in the current SD1D model by using a fraction of H^- density ($\frac{n_{H^-}}{n_{H_2}}$) as a function of T_e and n_e [18].
In the next section, the rate coefficients of collisional reactions and the hydrogen emissivity of five excitation channels (except ${H_3}^+$) will be discussed.

C. Analysis of collisional and radiative reactions with open databases

A number of collisional and radiative reactions occur in the tokamak edge and divertor, and greatly affect transport processes. A number of public databases provide the molecular reaction rate coefficients, e.g. the EIRENE or ADAS databases [18][20]. Even though ADAS is now one of the most reliable databases for studying atomic processes, it does not contain any data related to molecular species. We are employing it to provide impurity emissivity in the SD1D simulations, by using the impurity model '*atomic++coronal*' [19][20]. The EIRENE code has attached another database, which has been widely used in fusion numerical study, i.e. SOLPS[27], EDGE2D[13] and EMC3[28]. Amjuel[18] and Hydhel[29] are the two main parts of such a database, both of which contain extensive information on atomic and molecular reactions (including cross-sections, rate coefficients and population coefficients). While the reaction rate coefficients of ionisation, recombination, charge exchange, dissociation et al, are just a function of T_e in Hydhel, Amjuel presents a double polynomial fitting function of both T_e and n_e. Allowing for n_e variations, has a profound effect on the calculations. To further compare the two databases, the rate coefficients of the plasma-neutral collisional reactions were plotted and compared in the Appendix. In the upgraded SD1D simulations, all the reaction rate coefficients and hydrogen emissivity are obtained from Amjuel.

1. The rate coefficients of hydrogen atomic and molecular reactions

The rate coefficients for the reactions shown in Table 1 for both hydrogen atom and molecule are shown in figure C.1-C.3 as a function of electron temperature T_e. Each reaction has three curves, which represents the rate coefficient in three different electron densities: $n_e = 5 \times 10^{18}/m^3$, $n_e = 5 \times 10^{19}/m^3$ and $n_e = 5 \times 10^{20}/m^3$. In figure C.1, the ionisation, charge exchange and recombination rate coefficients show the basic processes occurring during divertor detachment: (1) ionisation and charge exchange are the dominant atomic processes at higher T_e; (2) once T_e goes down ($T_e < 10eV$), the ionisation rate coefficient drops, and charge exchange becomes the most significant atomic process; (3) recombination becomes more significant at $T_e < 1eV$. The effective volume ionisation and recombination rates are affected by both the rate coefficients and hydrogen atom fraction, both of which are crucial factors to trigger divertor detachment. In figure C.2, the rate coefficient curves shows non-dissociative ionisation is the main molecule sink at high temperatures, with dissociation contributing more when $T_e \sim 10eV$. Once $T_e < 10eV$, both dissociation rate coefficient and non-dissociative ionisation rate coefficient dramatically decrease, and molecular charge exchange gradually becomes the main molecule sink ($T_e \sim 2.0eV$).

$H_2{}^+$ is an important product from molecule collisional reactions. There are three channels for the dissociation of $H_2{}^+$: dissociative excitation ($e + H_2{}^+ \rightarrow e + H^+ + H$), dissociative ionisation ($e + H_2{}^+ \rightarrow e + H^+ + H^+$) and dissociative recombination ($e + H_2{}^+ \rightarrow e + H + H$). Through comparing the rate coefficients in figure C.3 to the coefficients of non-dissociative ionization and molecular charge exchange in figure C.2, the rate at which $H_2{}^+$ is dissociated is generally larger than the rate at which $H_2{}^+$ is produced, therefore the density of $H_2{}^+$ is always small. The density ratio $\frac{n_{H_2{}^+}}{n_{H_2}}$ is about 0.01 in the electron temperature range $1eV < T_e < 10eV$.

During the detachment discharge with fueling in divertor, molecules can be injected into the divertor volume by localized gas puffing, but it is typically recycling the main process that generates molecules near target. As molecular density increases, more $H_2{}^+$ will be produced and thus the $H_2{}^+$ collisional reactions will become more important. As a result, in such conditions this charged molecule plays a bigger role in the dynamics of detachment. The molecular activated recombination (MAR) via H^- channel is less important than the $H_2{}^+$ channel due to the relatively small rate coefficient as shown in Figure C.3.

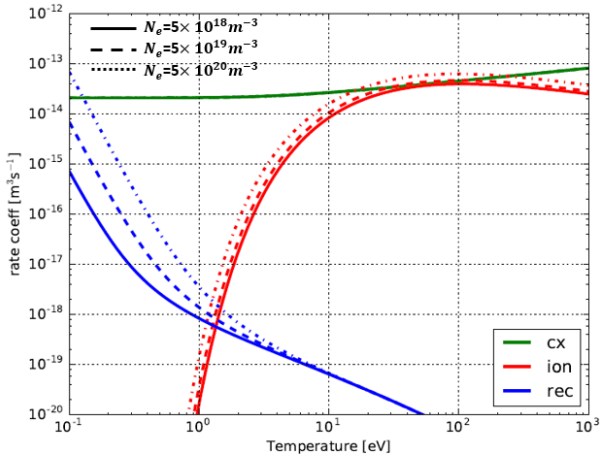

Figure C.1: Hydrogen atom effective ionisation, charge exchange and recombination rate coefficients as a function of electron temperature for electron density $n_e = 5 \times 10^{18}/m^3$, $n_e = 5 \times 10^{19}/m^3$ and $n_e = 5 \times 10^{20}/m^3$.

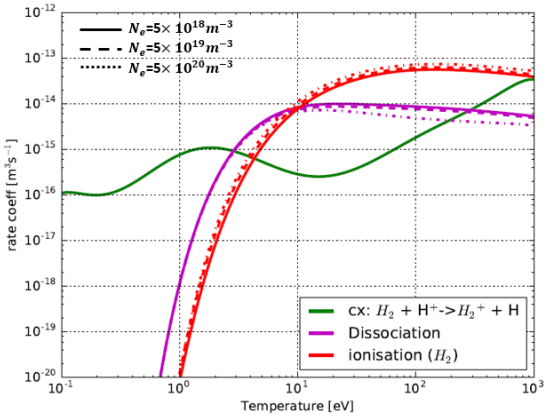

Figure C.2: Hydrogen molecule effective charge exchange, dissociation, and non dissociative ionisation rate coefficients as a function of electron temperature for electron density $n_e = 5 \times 10^{18}/m^3$, $n_e = 5 \times 10^{19}/m^3$ *and* $n_e = 5 \times 10^{20}/m^3$.

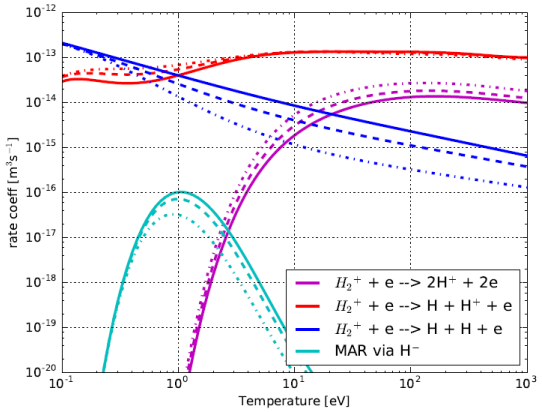

Figure C.3: Rate coefficients of effective dissociative ionisation (purple), dissociative excitation (red), dissociative recombination (blue) and molecular activated recombination (MAR) via H^-, *as a function of electron temperature for electron density* $n = 5 \times 10^{18}/m^3$, $n_e = 5 \times 10^{19}/m^3$ *and* $n_e = 5 \times 10^{20}/m^3$.

2. Analysis of hydrogen atomic and molecular excitations with Amjuel database

The emissivity $L = Pow_{pq}/N_e N_0$ (in $\text{erg} * \text{cm}^3 s$) corresponding to the low-n and medium-n Lyman lines (e.g n=2-6) are shown in figure C.4 for direct excitation (via H) and recombination (via H^+), dissociation (via H_2), dissociative recombination (via $H_2{}^+$) and mutual neutralization (via H^-) at three different electron densities. As mentioned in section B-2, the radiative reactions always happen together with the corresponding collisional reactions. Qualitatively, the curves of the ionisation rate coefficient and recombination rate coefficient shown in figure C.1 is similar as the corresponding emissivity curves in figure C.4 (a)-(c) and the corresponding the photon emission coefficients (e.g. Balmer lines n=3-6) shown in figure 5(a). Similarly, the curves of emissivity and Balmer photon emission coefficient via dissociation channel (H_2) and dissociative recombination channel ($H_2{}^+$) correspond to the rate coefficients of dissociation in figure C.2 and dissociative recombination in figure C.3, respectively. For the mutual neutralization excitation channel (H^-), its emissivity curve is similar as the rate coefficient of reaction 7.2.3b ($H^+ + H^- \rightarrow H^+ + H + 2e$) in Amjuel [18].

Looking at the emissivity of the hydrogen excited atom at different energy levels $(n = 2 - 6)$, it can be seen that the deviation between the curves via direct excitation is much larger than the

one between the recombination emissions. Therefore, the intersection of emissivity for the two excitation channels is located at a larger T_e for a higher-n Lyman line. Once the electron density increases, the direct excitation emissivity is slightly reduced, while the emissivity via recombination emission increases. Thus, the emission via recombination channel tends to be more significant at higher densities. Moving now to molecular emission, in figure C.4(d)-(f), the emissivity variation between different Lyman lines is generally large for the three excitation channels considered. Only the emissivity of the Lyman line n = 3 via $H_2{}^+$ and H^- does slightly decrease with the increase of electron density, while the others change little. One thing should be noted for the molecular excitation channels: due to the small densities, the excitation via $H_2{}^+$ and H^- are less important at high temperatures, even though the emissivity via $H_2{}^+$ and H^- is greater than the other channels, but they may become crucial in the divertor as their densities greatly enhance with the drop of temperature ($T_e < 3$eV) or with external fuelling (gas puffing). The photon emission via $H_2{}^+$ and H^-channel may also become important when $T_e < 3$eV , as the emission coefficients shown in figure C.5(b). In particular of H_{alpha} photon emission ($B_{3\to2}^{exc}$), $H_2{}^+$ and H^- are expected to the dominant excitation channels.

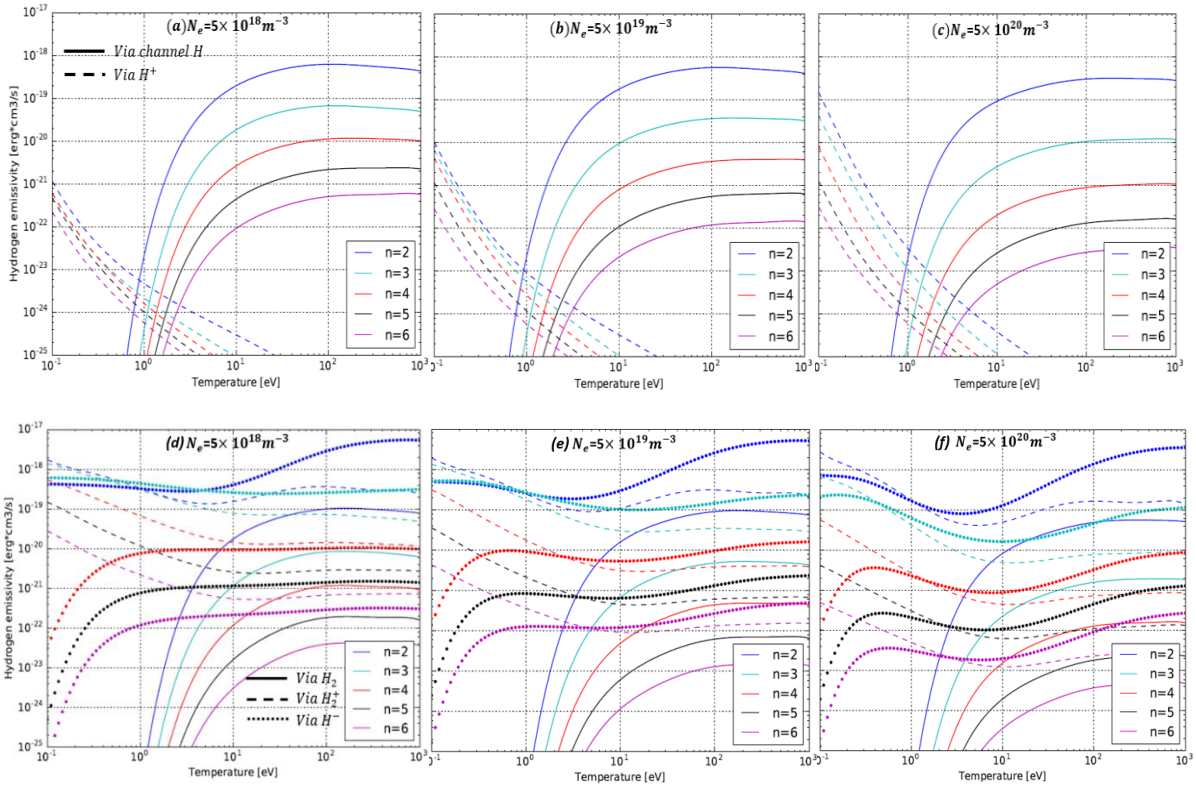

*Figure C.4: Hydrogen emissivity of the hydrogen excited atom at different energy levels (*Lyman lines $n= 2-6$*) as a function of electron temperature for the electron density $n_e = 5\times10^{18}/m^3$, $n_e = 5\times10^{19}/m^3$ and $n_e = 5\times10^{20}/m^3$. Two atomic excitation channels (direct excitation H and recombination H^+) and three molecular excitation channels (dissociation via H_2, dissociative recombination via $H_2{}^+$ and mutual neutralization via H^-) are shown here.*

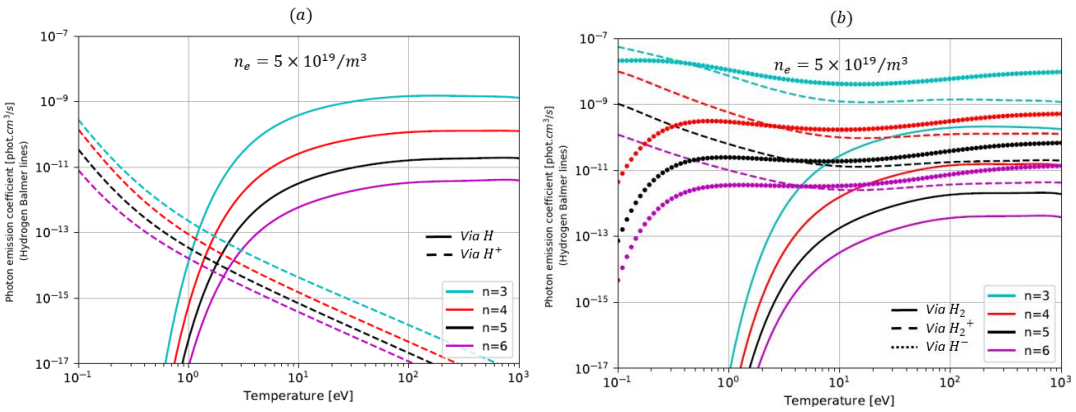

Figure C.5: Photon emission coefficient of the hydrogen excited atom at different energy levels (Balmer lines n= 3 − 6) as a function of electron temperature for the electron density $n_e = 5 \times 10^{19}/m^3$. (a) Two atomic excitation channels and (b)three molecular excitation channels are shown here.

D. A comparison of divertor detachment with and without hydrogen molecules

Investigating the behaviour of the particle flux Γ towards divertor target is a useful way to define the plasma detachment in both numerical and experimental research. We study here the rollover of Γ_{target} in all our scans, which include upstream density and upstream power flux. We compare the target particle flux to investigate the effects of molecules during detachment discharge with 1% carbon. All the simulations are implemented in MAST-Upgrade like conditions: (1) the parallel heat flux is $50MW/m^2$ at the X-point; (2) the connection length is 30m (20 m from X-point to target); (3) the effect of gradients in total magnetic field is considered with an area expansion factor (the ratio of $\frac{Total\ field\ at\ X-point}{Total\ field\ at\ target}$) of 2 between X-point and target [15]. 99% of plasma ion flux arriving at the target is recycled for all the cases considered. At the target, ions can recycle as both atoms or molecules, their relative ratio depending on the target material (and to a lesser extent, conditions). Here we include both recycling channels by changing such a ratio in a way that either atoms or molecules prevail. We have approached the problem by choosing three cases: one with just molecules as the recycling output, another with just atoms and a third with ions recycling as atoms or molecules with equal probability. The recycling temperature of neutral molecule and neutral atom is $T_{H_2,recycle} = 0.1eV$ and $T_{H,recycle} = 3.5eV$ in our simulations.

We start with an upstream density scan for the cases without hydrogen molecules H_2, as shown in figure D.1. Here we will compare a case with and without carbon impurities. The results show that the plasma ion flux towards target rolls over at an upstream density n_{up}~$1.8 \times 10^{19}/m^{-3}$ for the case without carbon (labelled 'H'), while including 1% carbon (labelled 'H & $carbon$'), the rollover occurs at a lower n_{up} (about $1.69 \times 10^{19}/m^{-3}$). Before the flux rollover, the influence of carbon impurity radiation is limited, but it gradually becomes significant after the rollover since both the plasma ion and carbon impurity accumulate near target with the increase of n_{up}. Therefore, the carbon impurity radiation greatly increases in the cases with a higher n_{up} and leads to a lower target temperature.

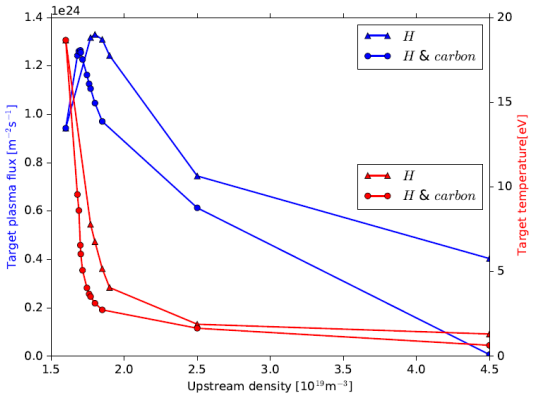

Figure D.1 Upstream density scan for the cases (a) without impurity and hydrogen molecule (labelled 'H'), (b) with 1% carbon impurity (labelled 'H & carbon')

The other two recycling channels, $H^+ \rightarrow H$ and $H^+ \rightarrow H_2$ in even proportions and only molecules, are considered in figure D.2. When molecules are introduced in the calculation, it is found that the flux rollover occurs at a higher n_{up} (varied from $1.69 \times 10^{19}/m^{-3}$ to $1.92\times 10^{19}/m^{-3}$) with a larger peak target flux, while the target temperatures before rollover gradually become higher. The reason is that the generation of hydrogen molecules from recycled ions reduces the source of atom, therefore causes a lower direct excitation radiation power and slows the atom-plasma interactions, which are the main energy sink before rollover in the divertor. In the case where the rollover occurs (e.g. the case at $n_{up} = 1.92 \times 10^{19}/m^{-3}$ in figure D.2), the ratio of total amounts of molecule and atom ($\frac{\int n_m dV}{\int n_n dV}$) in the divertor could be up to 50% when all recycled plasma ions become molecules. As shown in figure D.3, the reduction of atom source from recycling can lead to a much smaller peak atom density near the target, such that the peak density of plasma ion near the target is also gradually reduced. The plasma-neutral collisional and radiative interactions are, therefore, mitigated. Furthermore, the density profiles of H^+, H, H_2 and ${H_2}^+$ in figure D.3 indicate the plasma ion flux towards target first interacts with neutral atoms and the ion density dramatically decreases before hitting the molecule cloud (H and ${H_2}^+$) near the target. Due to the lower plasma density and temperature near the target, the molecular emission radiation is found to be much smaller than the atomic emission radiation, which accounts for over 85% of hydrogen emission radiation power in the divertor. After the rollover which marks divertor detachement in figure D.2, the plasma ion flux reaching target starts dropping with increasing n_{up}. As the recycling flux is proportional to the ion flux at the target, molecule densities are found to quickly rise at the beginning of detachment and then slowly drop with upstream density increasing further, while more atoms are produced by recombination (when $T_e < 1eV$) in the divertor. Hence, the molecule-plasma interactions might be less important than atom-plasma interactions in the divertor. The details about the effects of different reaction types on plasma momentum loss are discussed in figure D.8.

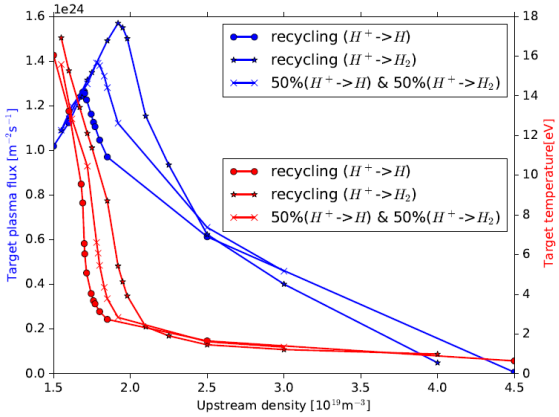

Figure D.2 Upstream density scan for the cases (a) with 1% carbon impurity and without molecules labelled 'recycling ($H^+ \rightarrow H$)', (b) with 1% carbon and hydrogen molecules (All recycled ions becomes molecules in this case), labelled 'recycling ($H^+ \rightarrow H_2$)', and (c) with

1% carbon and hydrogen molecules (half recycled ions becomes molecules and half becomes atoms in this case), labelled '50% ($H^+ \rightarrow H_2$) & 50% ($H^+ \rightarrow H$)'.

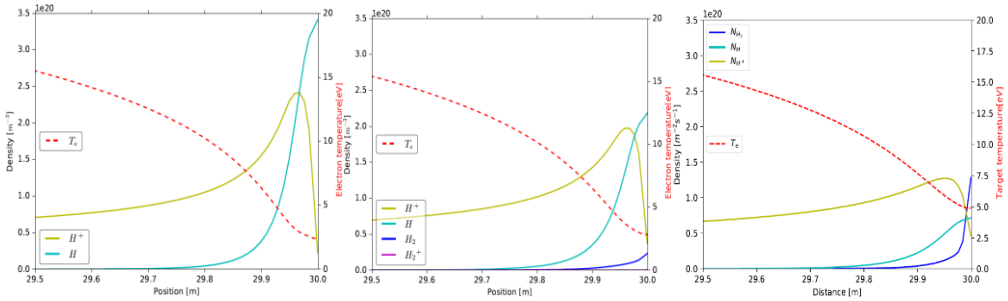

(a)100% ($H^+ \rightarrow H$) *(b) 50% ($H^+ \rightarrow H_2$) & 50% ($H^+ \rightarrow H$)* *(c)100% ($H^+ \rightarrow H_2$)*

*Figure D.3 Density profiles of H^+, H, H, $H_2{}^+$*and temperature profile of electron in the case with (a) all the recycled ions converting into atoms ($H^+ \rightarrow H$), (b) 50% recycled ions becoming atoms and the other half becoming molecules (*'50% ($H^+ \rightarrow H_2$) & 50% ($H^+ \rightarrow H$)'*, and (c) all the recycled ions converting into molecules ($H^+ \rightarrow H_2$). The upstream density is $n_{up} = 1.92 \times 10^{19}/m^{-3}$ for all the three cases, corresponding to the three cases at $n_{up} = 1.92 \times 10^{19}/m^{-3}$ in figure D.2. The target is located at the position of 30m.

Our calculations also allow us to get insight into the dissipation mechanisms at play. According to the Two Point Model (TPM), the upstream and target pressure should be such that $p_{up} = 2p_{target}$, if no momentum losses are considered. However, in the presence of plasma-neutral interactions, the plasma momentum will be affected and vary along the SOL. To keep into account this effect, a momentum loss factor is defined as:

$$f_m = 1 - 2p_{target}/p_{up} \qquad (9)$$

Before the code upgrade, the studies with SD1D in the same MAST-U like conditions [15], found that the factor could be written as an exponent function:

$$\frac{2p_{target}}{p_{up}} = 1 - f_m = 0.9[1 - e^{\left(-\frac{T_{target}}{2.1}\right)}]^{2.9} \qquad (10)$$

According to the Self-Ewald model [15][30], the atom-ion charge exchange imposes a drag force on the plasma ion momentum, while ionisation produces plasma ions. This mechanism for momentum losses is determined by the competition between ionisation and charge exchange, but it ignores many other factors, e.g. molecule-plasma interactions. The Self-Ewald model sets the momentum loss factor as a function of ionisation and charge exchange rate coefficients [30]: $1 - f_m = [\frac{\alpha}{\alpha+1}]^{(\alpha+1)/2}$, where $\alpha = <\sigma v>_{ion}/(<\sigma v>_{ion} + <\sigma v>_{cx})$. In the new version of SD1D used here, we could calculate the momentum loss factor based on the direct interaction with the atomic and molecular species. As a consequence, we can plot $\frac{2p_{target}}{p_{up}}$ from the cases previously discussed is in figure D.5, with the data well fitted by an exponential expression for the momentum loss factor (the black solid line):

$$\frac{2p_{target}}{p_{up}} = 1 - f_m = 0.889[1 - e^{\left(-\frac{T_{target}}{2.62}\right)}]^{1.65}. \qquad (11)$$

Having the target pressure from the expression above, we can now calculate the target particle flux: $\Gamma_{target} \propto n_{target}\sqrt{T_{target}} = p_{target}/\sqrt{T_{target}}$. Using the target pressure $p_{target} = \frac{(1-f_m)p_{up}}{2}$ from eq. 9, Γ_{target} can be written as:

$$\Gamma_{target} = p_{up}\frac{(1-f_m)}{\sqrt{8m_i T_{target}}} \qquad (12)$$

A target temperature scan at fixed p_{up} for the target plasma flux is shown in figure D.6, which compares the simulations to the analytical calculations obtained by replacing our expressions for $(1 - f_m)$ into eq. 12. To complement figure D.2, it is interesting to visualize our results in a Γ_{target} versus target temperature plot, which is shown in Figure D.6. What we see is that the detachment roll over occurs for all simulations at around 5eV regardless the specific recycling conditions. We could see that also eq. 12

together with the exponential expression in eq.11 give a curve for Γ_{target} that rolls over at a fixed target temperature as long as p_{up} does not vary much with the target temperature. To be more specific, we observe a small variation of the plasma temperature at rollover, with higher values (6.7eV) for recycling of pure atoms and smaller values (5.3eV) for pure molecular recycling.

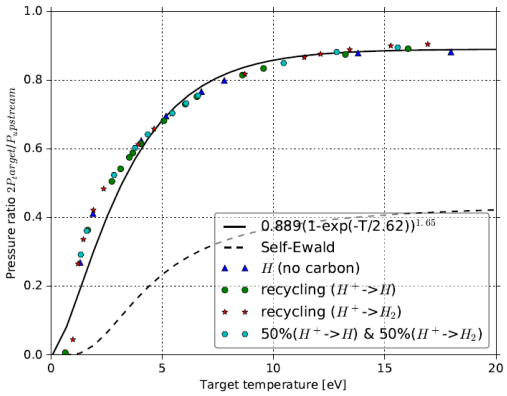

Figure D.5 Ratio of $\frac{2p_{target}}{p_{up}}$ as a function of target temperature achieved from the simulation cases without molecules (labelled 'H (no carbon)' and 'recycling ($H^+ \rightarrow H$), with molecules introduced by different recycling conditions (labelled 'recycling ($H^+ \rightarrow H_2$)' and '50% ($H^+ \rightarrow H_2$) & 50% ($H^+ \rightarrow H$)')

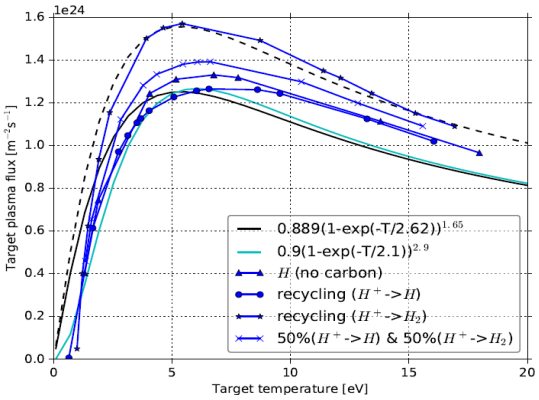

Figure D.6. Target flux as a function of target temperature for the upstream density scan in the cases: 1) without impurity and molecules labelled 'H (no carbon)', 2) with 1% carbon and without molecules labelled 'recycling ($H^+ \rightarrow H$)', 3) with 1% carbon and with hydrogen molecules labelled 'recycling ($H^+ \rightarrow H_2$)' and '50% ($H^+ \rightarrow H_2$) & 50% ($H^+ \rightarrow H$)'. The celeste and black solid curves show the target flux calculated with eq. 12 by using eq. 10 and eq. 11. The upstream density is $n_{up} = 1.97 \times 10^{19}/m^{-3}$ for the black and celeste solid lines, while $n_{up} = 2.35 \times 10^{19}/m^{-3}$ for the black dashed line.

Part of the the input power P_{in} is dissipated by the impurity radiation P_{imp}, part used to ionise the neutrals in the target region P_{ion} and the rest, P_{target}, reaches the target. According to [2], we define

$$P_{recl} = P_{ion} + P_{target} = (E_{ion} + \gamma T_{target})\Gamma_{target}, \qquad (13)$$

where $\gamma T_{target}\Gamma_{target}$ represents the total energy density reaching target and E_{ion} is the total effective ionisation energy (including hydrogen excitation). Together with the eq.12, the detachment parameter $\frac{p_{up}}{P_{recl}}$ (p_{up} represents upstream pressure) could be obtained:

$$\frac{p_{up}}{P_{recl}} = \frac{\sqrt{8m_i T_{target}}}{(1-f_m)(E_{ion}+\gamma T_{target})} \qquad (14)$$

$$= \frac{\sqrt{8m_i\gamma}\, E_{ion}^{-\frac{1}{2}}\left(\frac{\gamma T_t}{E_{ion}}\right)^{\frac{1}{2}}}{(1-f_m)\left(1+\frac{\gamma T_t}{E_{ion}}\right)}$$

,

where $1-f_m=\frac{2p_{target}}{p_{up}}$ is a function of target temperature as shown in eq.11. Thus, both the target temperature and the effective ionisation energy E_{ion} at the time when rollover occurs determine the detachment threshold $\frac{p_{up}}{P_{recl}}$. According to figure D.4, $1-f_m$ varies little when $T_t > 10eV$, and steeply go to zero when $T_t < 10eV$. If a fixed ionisation energy is used in calculation, $\frac{p_{up}}{P_{recl}}$ grows as the target temperature decreases (dashed line in figure D.7). We can absorb the effect of neutral radiation in the ionization energy in an ad hoc way, which is an approximation that is sometime used to capture both effects. If we do so, E_{ion} becomes a function of the target temperature, which now would represent the total energy loss of ionisation plus hydrogen atom excitation divided by the ionisation rate. We have shown this quantity as a red solid line in figure D.7, by using our numerical results from the simulation with pure molecular recycling. We have found that the other simulations with different recycling conditions produced simila results. Using this in (14), we find that the ratio of $\frac{p_{up}}{P_{recl}}$ is about *9.5N/MW* at high temperatures, and it quickly decreases when $T_t < 10eV$, as the blue solid line shows in figure D.7. Generally, the target flux rollover, indicating onset of detachment, occurs when a critical value of the gradient of E_{ion} with respect to T_t is achieved [2][15][25]:

$$\frac{\partial E_{ion}}{\partial T_t} < -\gamma, \qquad (15)$$

For the sheath transmission coefficient γ used in this paper (γ =6), we find $T_t = 5.6eV$ and the corresponding effective ionisation energy $E_{ion} = 82.23eV$. This corresponds to the value of the detachment parameter given below:

$$\frac{p_{up}}{P_{recl}} = 8.1\ N/MW,$$

which is smaller than 12.6N/MW found in the old SD1D [15] and 17N/MW found in SOLPS4.3 simulation on DIII-D like equilibria [31]. However, it is similar to the measured value of $\frac{p_{up}}{P_{recl}}$ on TCV (#56567), which shows the detachment threshold is between 5 N/MW and 10 N/MW when the target flux rollover occurs [25].

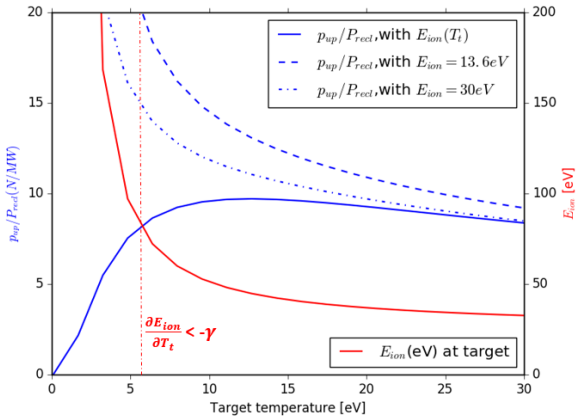

Figure D.7. $\frac{p_{up}}{P_{recl}}$ *as a function (eq.14) of target temperature and effective ionisation energy* E_{ion} *.* $\frac{p_{up}}{P_{recl}}$ *is calculated with fixed* $E_{ion} = 13.6eV, 30eV$ *and with the* $E_{ion}(T_t)$ *as a function of target temperature (which is the total energy loss of ionisation and hydrogen atom emission divided by the ionisation rate as the red solid line shows). The threshold in eq.15 is marked by the vertical red dashed line.*

As discussed in some previous works [11][25], plasma ions can undergo charge exchange collisions with hydrogen molecules ($H^+ + H_2 \rightarrow H_2{}^+ + H$) in the divertor, which may account for a rise of plasma ion momentum loss in the low temperature region. To investigate the importance of molecule-plasma charge exchange and other reaction types, we use a momentum loss factor $f_{momloss} = (\sum_p \int_{up}^{target} F_{H^+-p} dl)/p_{up}$, where $\sum_p \int_{up}^{target} F_{H^+-p} dl$ is the total energy loss of H^+ by the collisions with other particle species 'p' (F_{H^+-p} represents collision force). Based on SD1D simulations (the case of *'recycling* ($H^+ \rightarrow H_2$)*'*),

we found molecule density near the target enhances quickly at the onset of detachment ($n_{H_2} > n_H$ at this moment), and thus it is found that in figure D.8(a) the momentum loss $f_{momloss}$ caused by H_2 - H^+ rises rapidly and it becomes more important than other collisions when $n_{up} < 2.2 \times 10^{19}/m^{-3}$. But with the n_{up} growing further, the growth of molecule density becomes slower and molecule density is even found to decrease at high upstream densities ($n_{up} > 3.5 \times 10^{19}/m^{-3}$) due to the decreasing recycling source (plasma ion flux at the target Γ_{target}) and no external fuelling included. In a result, H_2 - H^+collisions becomes less important, while H - H^+ collisions provide the largest part of momentum loss because recombination produces more neutral atoms at low temperatures ($n_{H_2} < n_H$ at this moment). In figure D.8(b), it compares the momentum loss caused by two main H_2 - H^+ interactions, charge exchange and elastic collision. The simulation result predicts that the momentum loss mechanism via H_2 - H^+ interactions is primarily due to H_2 - H^+ elastic collisions, instead of ion-molecular charge exchange.

H_{alpha} emission signal ($B_{3\to2}^{exc}$) is crucial for tokamak experiment diagnostic, which conveys information of neutral density and neutral-plasma interactions. In figure D.8(c), simulations found that atomic channels (primarily direct excitation) dominate H_{alpha} emission before Γ_{target} rollover and then change little during detachment, while molecular channels account for the strong rise of H_{alpha} signal, which grows to be 5 times of the H_{alpha} at Γ_{target} rollover ($n_{up} = 1.92 \times 10^{19}/m^{-3}$). It is mainly due to the fast growth of molecule density near target at the beginning of detachment and then due to the increase of H_{alpha} emission coefficients via dissociative excitation '$H_2{}^+$' and mutual nuetralization 'H^-' (figure C.5(b)) with the decrease of T_e when $T_e < 3.0eV$. This result well matches the measured and predicted photon emission on TCV [11]. Further analysis of the decomposition of molecular channels in figure D.8(d) shows the rise of H_{alpha} signal is firstly due to $H_2{}^+$ channel ($1.92 \times 10^{19}/m^{-3} < n_{up} < 2.5 \times 10^{19}/m^{-3}$) and then H^- channel becomes more important when the target gets further detached ($n_{up} > 2.5 \times 10^{19}/m^{-3}$).

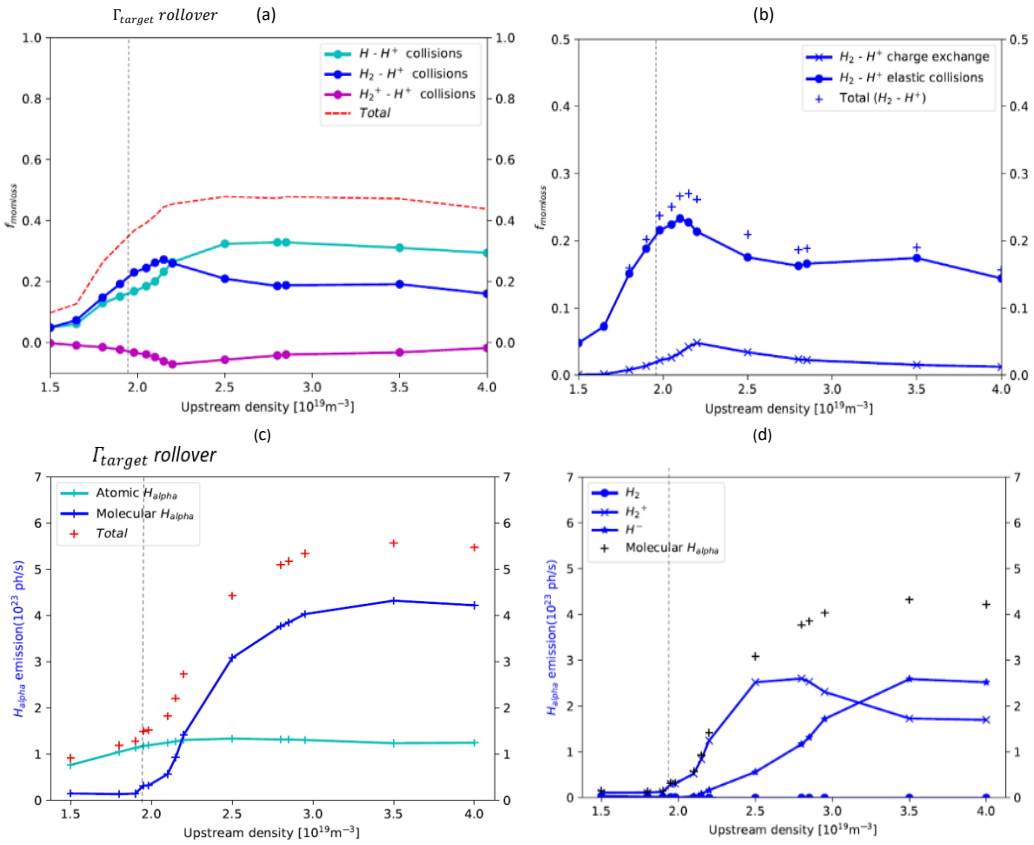

Figure D.8 (a) Decomposition of momentum loss factor $f_{momloss}$ due to different reaction types, labelled as 'H - H^+', 'H_2 - H^+', 'H_2^+ - H^+' collisions, and their total $f_{momloss}$ (the red dashd) when all recycled ions become molecules; (b) Decomposition of $f_{momloss}$ caused by H_2 - H^+collisions.(c)

decomposition of total H_{alpha} photon emission due to atomic and molecular channel, (d) decomposition of H_{alpha} photon emission through molecular channels. Vertical dashed lines indicates the position of Γ_{target} rollover.

E. Conclusions

In the previous version of SD1D, only atomic collisional and radiative reactions were included, while molecular processes were neglected. To better investigate the physics of divertor detachment, an important upgrade was carried out of the SD1D model by adding a molecule model, including a hydrogen molecule H_2 and charged molecule ${H_2}^+$ species. The Amjuel database is used to provide data of the molecular collisional and radiative reactions listed in Table 1.

Using the upgraded SD1D code in the MAST-Upgrade like conditions, we have studied the role of H_2 and ${H_2}^+$ in detached regimes of tokamak plasmas. It is found that molecules play an important role on the flux rollover, which occurs at a lower target temperature and a larger upstream density if a larger proportion of H_2 generated from recycling process.

Generally, the target flux rolls over, indicating onset of detachment, occurs when a critical value of the gradient of E_{ion} with respect to T_{target} is achieved: $\frac{\partial E_{ion}}{\partial T_t} < -\gamma$ [2][15]. For the sheath transmission coefficient $\gamma = 6$ used in this paper, we find $T_t = 5.6eV$ and the corresponding effective ionisation energy $E_{ion} = 82.23eV$ for flux rollover. In the simulations, we also calculated the momentum loss factor $f_m = 1 - 2p_{target}/p_{up}$ and obtained $\frac{2p_{target}}{p_{up}}$ as a function of target temperature: $\frac{2p_{target}}{p_{up}} = 1 - f_m = 0.889[1 - e^{\left(-\frac{T_{target}}{2.62}\right)}]^{1.65}$. This corresponds to the value of the critical detachment parameter (eq. 14) given as $\frac{p_{up}}{P_{recl}} = 8.1\ N/MW$, which is smaller than the value found by the previous version of SD1D [15] and close to the measured value on TCV [25].

The SD1D simulations predicts that both molecule–plasma and atom–plasma collisions can lead to a large plasma momentum loss during detachment. The decomposition of momentum loss shows molecule-plasma elastic collision dominates molecule-plasma interactions, while molecular charge exchange cannot effectively reduce plasma momentum. The H_{alpha} emission diagnostic is also considered in SD1D simulations, which found a strong rise of H_{alpha} signal when the upstream density is increased after rollover. The ${H_2}^+$ channel accounts for the most growth of H_{alpha} at the onset of detachment and then H^- channel contributes more when the target gets further detached.

F. Appendix

Figure F.1 shows the rate coefficients calculated by using Hydhel databases [29], which collect plenty of reaction cross-section and rate coefficient for hydrogen-helium plasma. As mentioned in section C-1, the main difference is that the rate coefficients of Hydhel are not related to the electron density, while rate coefficients are determined by both electron temperature and plasma density. A huge error will inevitably appear if Hydhel database is applied to study the divertor physics. With the increase of electron density in figure C.1, specifically, the rate coefficient greatly enhances at lower temperatures (e.g. $T_e < 5eV$), while no such change occurs in figure E.1(a). Thus, it may contribute a significant error to the hydrogen atom and plasma ion densities. Another crucial difference is that the rate coefficients of molecular charge exchange and dissociation in figure E.1(b) are about 1 order smaller than the results shown in figure C.2 at $T_e < 10eV$. It will largely reduce the molecule sink in simulations, and therefore narrows the source of charged molecule ${H_2}^+$. The dissociative excitation rate coefficient from Amjuel includes the component $e + {H_2}^+ \rightarrow H^* + H \rightarrow H^+ + H$, while the dissociative excitation rate coefficient from Hydhel consider $e + {H_2}^+ \rightarrow e + {H_2}^{+*} \rightarrow H^+ + H$ [18] [29]. H^* and ${H_2}^{+*}$ represent the excited atom and vibrational excited molecule. As discussed in section C-2, H_2 and ${H_2}^+$ just convert into the excited atom in this paper. Thus, the Amjuel database is applied to provide dissociative excitation rate coefficient in simulations.

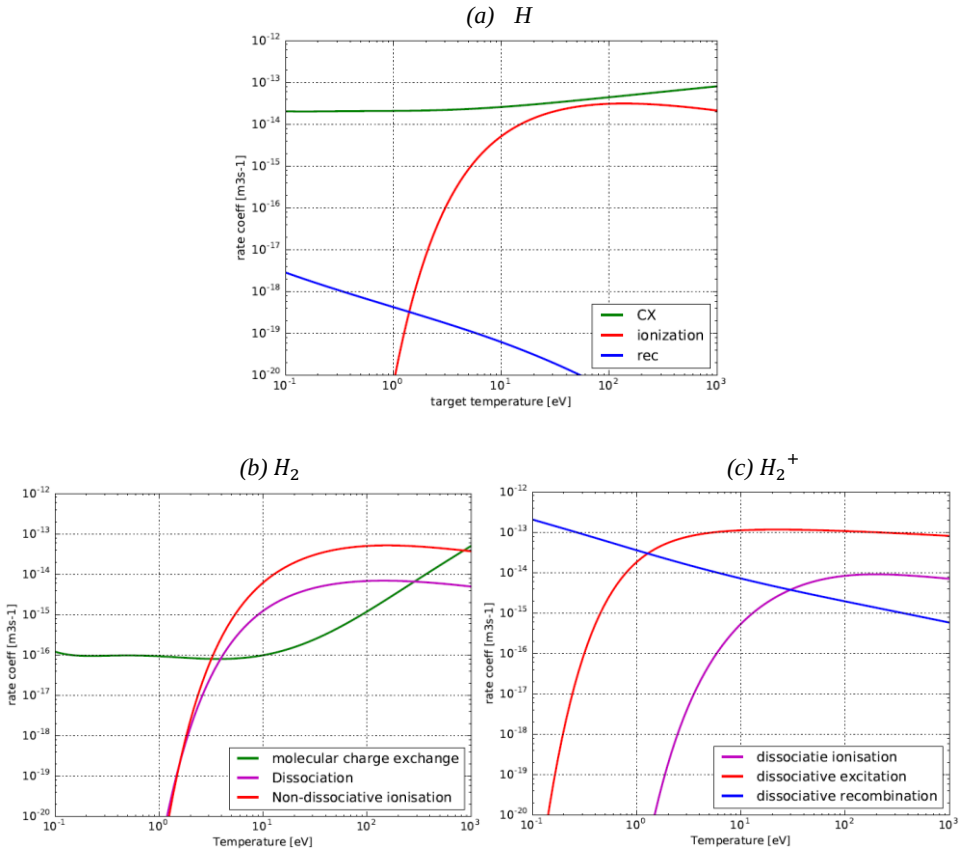

Figure F.1 The rate coefficients of collisional reactions related to (a) hydrogen atom H, (b) molecule H_2 and (c) charged molecule H_2^+, calculated by data from [29]

G. Ackownledge

This work has been (part-) funded by the RCUK Energy Programme [grant number EP/T012250/1], the China Scholarship Council (award to Yulin Zhou for a 3 year PhD programme at University of York), the National Science Foundation for Young Scientists of China (Grant No. 11805055), the Chinese ITER Project (2018YFE0303102) and CFETR project (2017YFE0302100). To obtain further information on the data and models underlying this paper please contact yz3138@york.ac.uk

H. References

[1]. A. Kallenbach, M. Bernert, R. Dux, F. Reimold, M. Wischmeier, and ASDEX Upgrade Team. Plasma Physics and Controlled Fusion, 58(4):045013, 2016
[2]. P. C. Stangeby, Plasma Physics and Controlled Fusion, 60(4):044022, 2018
[3]. H. J. Kunze, Introduction to plasma spectroscopy, volume 56. Springer, 2009
[4]. M. Bernert, M. Wischmeier, A. Huber, F. Reimold, B. Lipschultz, C. Lowry, S. Brezinsek, R. Dux, T. Eich, A. Kallenbach et al., Nuclear Materials and Energy, 12 111-118, 2017
[5]. Peter Stangeby. Plasma Physics and Controlled Fusion, 60(4):044022, 2018
[6]. S. I. Krasheninnikov, A. S. Kukushkin, and A. A. Pshenov, Phys. Plasmas, 23(5):055602, 2016
[7]. D. Moulton, J. Harrison, B. Lipschultz, and D. Coster, Plasma Physics and Controlled Fusion, 59(6):065011, 2017

[8]. I. Paradela Pérez, A. Scarabosio, M. Groth, M. Wischmeier, F. Reimold, and ASDEX Upgrade Team. Nuclear Materials and Energy, 12:181-186, 2017
[9]. I Bykov, D L Rudakov, A Yu Pigarov et al., Phys. Scr. T171 (2020) 014058
[10]. C. Zhang, C. F. Sang, L. Wang et al., Plasma Phys. Control. Fusion 61 (2019) 115013
[11]. K. Verhaegh, thesis, University of York, September 2018
[12]. H. L. Du, C. F. Sang, L. Wang, X. Bonnin, H. Y. Guo, J. Z. Sun and D. Z. Wang, Plasma Phys. Control. Fusion 58 085006, 2016
[13]. M. Groth, E. M. Hollmann, A. E.Jaervinen et.al, Nuclear Materials and Energy 19 211-217, 2019
[14]. S. I. Krasheninnikov and A. S. Kukushkin, J.Plasma Phys., 83:155830501, 2017.
[15]. B. Dudson, J. Allen, T. Body, B. Chapman, C. Lau, L. Townley, D. Moulton, J. Harrison and B. Lipschultz, Plasma Phys. Control. Fusion 61 (2019) 065008
[16]. M. Nakamura, S. Togo, M. Ito and Y. Ogawa, J. Plasma Fusion Res., 6:2403098, 2011
[17]. S. Togo et al. J. Plasma Fusion Res., 8:2403096, 2013
[18]. D. Reiter, The data file AMJUEL: Additional Atomic and Molecular Data for EIRENE, Version: January 13, 2020
[19]. T. Body, 'Simulating Radiative Cooling and Detachment in a Divertor Plasma', thesis submitted for degree of MSc, University of York 2017
[20]. H. P. Summers. The ADAS user manual, version 2.6, 2004.
[21]. E. Havlíčková, W. Fundamenski, F. Subba, D. Coster, M. Wischmeier and G. Fishpool, Plasma Phys. Control. Fusion, 55 065004, 2013
[22]. J. Leddy, B. Dudson and H.Willett, Nuclear Materials and Energy, 12:994-998,2017
[23]. D. Wunderlich and U. Fantz. Atoms, 4(4), 2016
[24]. NIST Standard Reference Database 78, Version 5.7, 2019. URL: https://dx.doi.org/10.18434/T4W30F
[25]. K. Verhaegh, Nuclear Materials and Energy, 12:1112-1117, 2017
[26]. V. Kotov, D. Reiter, A. S. Kukushkin, *Numerical study of the ITER divertor plasma with the B2-EIRENE code package*, Technical report, Forschungszentrums Juelich (Germany), Nov 2007; 142 p
[27]. Y.P. Chen, D.R. Zhang, S.C. Liu, G.S. Xu, L. Wang, D.M. Yao, Z.P. Luo, L.Q. Hu and EAST Team, Nucl. Fusion, 60: 036019 2020, URL: https://doi.org/10.1088/1741-4326/ab69e3
[28]. H. Frerichsa, X. Bonnin, Y. Feng, A. Loarte, R. A. Pitts, D. Reiter, O.Schmitz, Nuclear Materials and Energy, 18: 62-66, 2019
[29]. R. K. Janev, D. Reiter, U. Samm, Collision Processes in Low-Temperature Hydrogen Plasmas, Forschungszentrum, Zentralbibliothek Jülich 2003
[30]. S. A. Self and H. N. Ewald, Physics of Fluids, 09: 2486, 1966.
[31]. A. A. Pshenova, A. S. Kukushkina and S. I. Krasheninnikov, Nuclear Materials and Energy, 12:948-952, 2017